

Subsystem localization

Arpita Goswami,^{*} Pallabi Chatterjee,^{*} Ranjan Modak,[†] and Shaon Sahoo[‡]

Department of Physics, Indian Institute of Technology Tirupati, India, 517619

(Dated: June 9, 2025)

We consider a ladder system where one leg, referred to as the “bath”, is governed by an Aubry-André (AA) type Hamiltonian, while the other leg, termed the “subsystem”, follows a standard tight-binding Hamiltonian. We investigate the localization properties in the subsystem induced by its coupling to the bath. For the coupling strength larger than a critical value ($t' > t'_c$), the analysis of the static properties show that there are three distinct phases as the AA potential strength V is varied: a fully delocalized phase at low V , a localized phase at intermediate V , and a weakly delocalized (fractal) phase at large V . An analysis of the wavepacket dynamics shows that the delocalized phase exhibits a ballistic behavior, whereas the weakly delocalized phase is subdiffusive. Interestingly, we also find a superdiffusive narrow crossover regime along the line separating the delocalized and localized phases. When $t' < t'_c$, the intermediate localized phase disappears, and we find a delocalized (ballistic) phase at low V and a weakly delocalized (subdiffusive) phase at large V . Between those two phases, there is also a crossover regime where the system can be super- or subdiffusive. Finally, in some limiting scenario, we also establish a mapping between our ladder system and a well-studied one-dimensional generalized Aubry-André (GAA) model.

I. INTRODUCTION

Anderson localization is a key quantum effect where uncorrelated disorder localizes wavefunctions and blocks transport of non-interacting electrons [1–3]. It creates a mobility edge in three dimensions that separates localized and extended states. A metal-insulator transition occurs when the Fermi energy crosses this edge. In one dimension (1D), all states become localized with any amount of disorder. There is no mobility edge and no transition. Introducing interactions in such disordered Anderson localized systems can stabilize a many-body localized (MBL) phase, where systems fail to thermalize and retain memory of initial conditions [4–11]. This behavior contradicts the Eigenstate Thermalization Hypothesis (ETH), which posits that isolated non-integrable systems should relax to thermal equilibrium [12–15]. However, recent studies highlight the avalanche instability within the MBL phase. This instability suggests that rare regions of the system can thermalize and spread thermalization through the system, potentially destabilizing the MBL phase [16–18].

On the other hand, the presence of correlated disorder can significantly change the Anderson localization scenario in 1D. One can find the localization-delocalization transition and even the existence of the mobility edge, which is also feasible in such systems. One of the prime examples of such systems is the Aubry-André (AA) Hamiltonian, where the uncorrelated “true” disorder is replaced by a quasi-periodic potential [19]. One can induce a delocalization-localization transition by tuning the strength of the quasi-periodic potential, a phenomenon that holds significance in various physical contexts [20–24]. The AA Hamiltonian also has the unique

property of self-duality at the critical point, with identical real space and momentum space representations, thus it contains an energy-independent localization transition for the whole spectrum with no mobility edges. It has been shown that by adding different types of perturbations to the AA model, the fine-tuned AA duality conditions can be broken, and an energy-dependent self-duality relation can be established, automatically implying the existence of the mobility edges [25–32]. With the remarkable progress in cold-atom and ion-trap experiments over the past decade, many of these models have been experimentally realized [33–36], providing strong motivation to study quasi-periodic systems beyond purely theoretical interest. In this context, the emergence of a non-ergodic metallic phase has been proposed in models with single-particle mobility edges when interactions are introduced. [37–41]. One of the questions in the field of localization has persisted for some time now, i.e., what happens if one couples localized and extended systems together? In the case of a many-body interacting system, if the degrees of freedom of the extended system are large enough compared to the localized system, the extended system is expected to thermalize the localized one. On the other hand, if the delocalized degrees of freedom are comparable to the localized ones, the outcome is not yet clear. Many efforts have been made to address this question in the last several years [42–46]. Numerical challenges to tackle the exponentially growing Hilbert space dimension with system size and limitations of analytical tools to solve interacting systems have made this problem extremely challenging. This manuscript has tried to address a similar question in the non-interacting context.

We consider a ladder system where one leg, referred to as the “bath” B is a 1D non-interacting disordered chain, while the other leg, termed the “subsystem” A , is described by a clean delocalized tight-binding Hamiltonian (see the schematic of our system in Fig. 1). If

^{*} These authors contributed equally

[†] Contact author: ranjan@iittp.ac.in

[‡] Contact author: shaon@iittp.ac.in

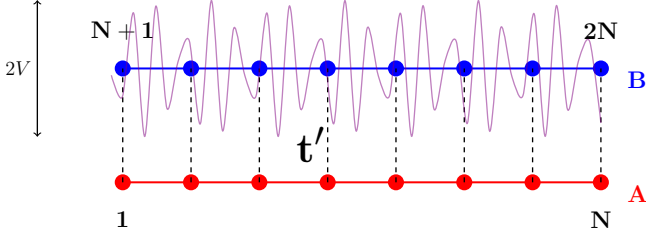


FIG. 1: Schematic diagram of the model: the subsystem (A) is described by a standard TB Hamiltonian whereas the bath (B) is governed by an AA type potential.

the disorder in bath B is uncorrelated, according to the rule of Anderson localization (i.e., any tiny disorder is sufficient to localize all states in 1D and 2D), both the subsystem A and Bath B of the total system are expected to be Anderson localized. However, if the disorder is correlated, the outcome is not at all apparent, given that the so-called rule of Anderson localization does not apply there. We investigate such a scenario by introducing a quasi-periodic potential in bath B . To be more precise, our B part of the system is described by the AA Hamiltonian (which undergoes a delocalization-localization transition with increasing the strength of the quasi-periodic potential). We find that, depending on the strength of the quasi-periodic potential V and the coupling strength t'_{AB} between subsystem A and bath B , it is possible to localize the subsystem. One might expect such a situation to arise (if at all) in the large V limit, when the bath B is strongly localized. Interestingly, it turns out that is not the case. In contrast, this situation arises when t'_{AB} is larger than a critical strength t'_c , and that too for an intermediate range of V . In the $V \gg t'_{AB}$ limit, the subsystem A remains (weakly) delocalized and displays subdiffusive transport.

II. MODEL SYSTEM AND PHASE DIAGRAM

In this section, we first describe the model system that we investigate. Next, we provide a summary of our results and present a schematic phase diagram.

A. Model system

In this paper, we investigate a ladder system whose one leg is called the “subsystem” and the other leg is called the “bath”. These are, respectively, indicated by “A” and “B” in the schematic diagram (Fig. 1). The subsystem A is described by a standard tight-binding (TB) Hamiltonian (H_A in Eq. 1) while the bath is governed by an Aubry-André (AA) type Hamiltonian (H_B in Eq. 1). Without the coupling ($t' = 0$) between the subsystem A and bath B , all the states in A are delocalized. The problem we investigate here is whether and when states

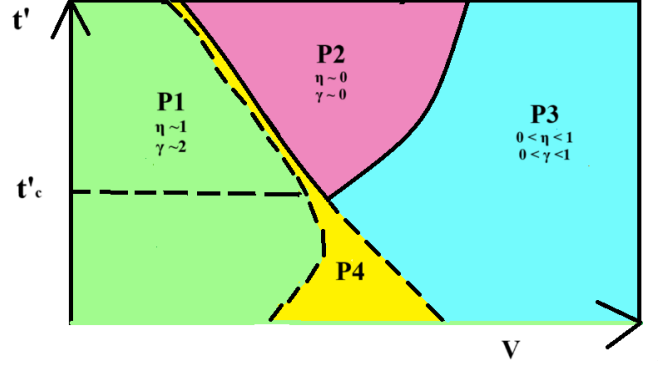


FIG. 2: Schematic phase diagram: P1 - delocalized (ballistic) phase, P2 - localized phase, P3 - weakly delocalized (fractal and subdiffusive) phase, and P4 - a crossover regime (above t'_c it is superdiffusive, and below t'_c it is super- or subdiffusive).

become localized in A as we establish a coupling ($t' \neq 0$) between A and B .

The full Hamiltonian of the ladder system appears in the following equation:

$$\begin{aligned}
 H &= H_A + H_B + H_{AB}, \text{ where} \\
 H_A &= -t_A \sum_{j=1}^{N-1} (c_j^\dagger c_{j+1} + hc), \\
 H_B &= -t_B \sum_{i=N+1}^{2N-1} (c_i^\dagger c_{i+1} + hc) \\
 &\quad + V \sum_{i=N+1}^{2N} \cos(2\pi\beta i + \phi) c_i^\dagger c_i, \text{ and} \\
 H_{AB} &= -t'_{AB} \sum_{j=1}^N (c_j^\dagger c_{N+j} + hc).
 \end{aligned} \tag{1}$$

We take $t_A = t_B = 1$ and $\beta = \frac{\sqrt{5}-1}{2}$. For our numerical study, we take V and t'_{AB} as two parameters. The second parameter t'_{AB} will be denoted by t' in the remainder of the paper. We do ϕ averaging for all our results for better statistics.

B. Phase Diagram

The summary of our main results is presented in the schematic diagram of Fig. 2. The study of the static properties, as discussed in Sec. III, reveals that above a certain threshold value of the coupling strength ($t' > t'_c$), we have three distinct phases - a fully delocalized phase (for small values of V), a fully localized phase (for intermediate values of V) and a weakly delocalized (fractal) phase (for large values of V). We see a narrow crossover region with fractal character. The study of wavepacket

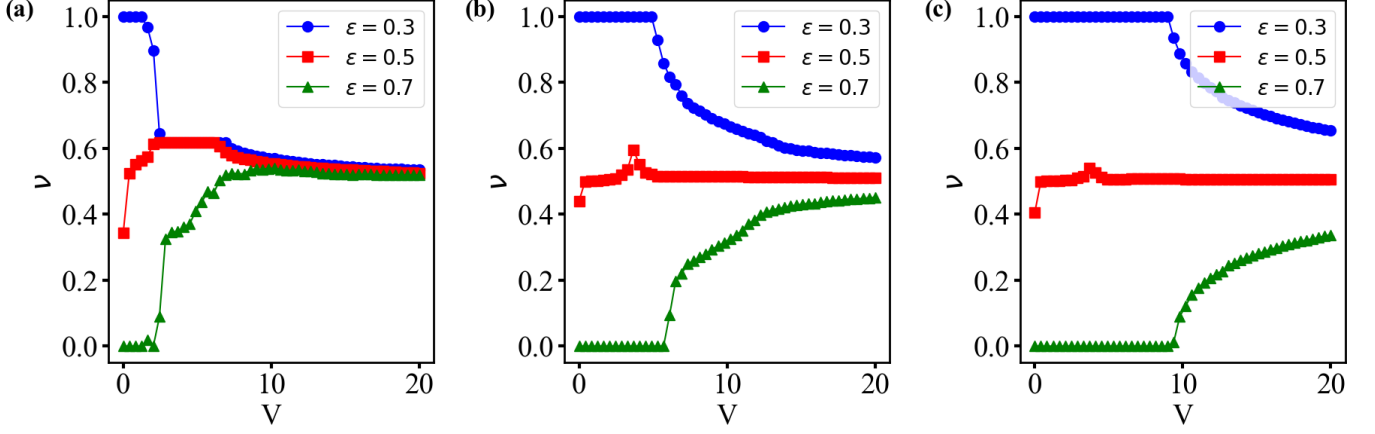


FIG. 3: (a)-(c): ν vs. V plots for $t' = 1, 5$ and 10 , respectively. The calculations are performed for the total subsystem size $N = 500$.

dynamics, as discussed in Sec. IV, reveals that the delocalized phase is ballistic and the weakly delocalized phase is subdiffusive in nature. Interestingly, the crossover region is found to be superdiffusive in nature.

In the regime where $t' < t'_c$, the study of static properties shows the absence of the localized phase. Here, one finds two phase - a delocalized phase for small values of V and a weakly delocalized (fractal) phase for large value of V . The study of wavepacket dynamics reveals that there is some intermediate crossover regime which is a fractal phase but can be super- or subdiffusive in nature.

It may be worth noting here that the phase diagram presented here strongly depends on the nature of the potential in the bath B . Instead of correlated AA type potential, if we take a random potential (for example, replace the uniform phase factor ϕ in Eq. 1 by a site-dependent uncorrelated phase factor ϕ_i), the subsystem A will always be in a localized phase, in accordance with the Anderson localization in a disordered one-dimensional system. The relevant result is presented in Fig. 13.

III. STATIC PROPERTIES

In this section, we study the localization properties of the subsystem A , as a function of the coupling strength t' and the AA potential strength V . For this purpose, we calculate the Inverse Participation Ratio for the subsystem (denoted by IPR_A) and the average Participation Ratio for the subsystem (denoted by $\langle PR_A \rangle$). To evaluate IPR_A , we first project an eigenket of the full Hamiltonian (Eq. 1) onto the subsystem A . We then calculate IPR_A from the normalized projected state. If $|\xi_n\rangle$ is the n th eigenket of the full Hamiltonian, and \hat{P}_A is the projector for the subsystem A , the corresponding

normalized projected state for the subsystem is:

$$|\psi_n\rangle = \frac{\hat{P}_A |\xi_n\rangle}{\|\hat{P}_A |\xi_n\rangle\|} = \frac{\sum_{j=1}^N \langle j | \xi_n \rangle |j\rangle}{\|\sum_{j=1}^N \langle j | \xi_n \rangle |j\rangle\|}. \quad (2)$$

It may be noted here that we choose the standard site basis $\{|j\rangle\}$ for our calculations, where $|j\rangle$ represents a ket corresponding to a single particle at the j th site (and no particles at any other site). We define the subsystem IPR in the following way:

$$IPR_A^{(n)} = \sum_{j \in A} |\langle j | \xi_n \rangle|^4, \quad (3)$$

where n is the eigenket index.

It is worth noting here that all the eigenkets of the full Hamiltonian do not have the same degree of significance when studied from the subsystem A . To study the localization on the subsystem A , we only analyze those eigenkets for which the subsystem probability p_A is larger than certain value (ϵ), where

$$p_A = \sum_{j \in A} |\langle j | \xi \rangle|^2, \quad (4)$$

for an eigenket $|\xi\rangle$ of the full Hamiltonian. An eigenket is called an ϵ -significant if $p_A \geq \epsilon$. For $\epsilon = 0.3, 0.5$ and 0.7 , we calculate and analyze IPR_A and $\langle PR_A \rangle$ (defined later) of the ϵ -significant eigenkets.

To see how many eigenkets are ϵ -significant for the subsystem A , we define a parameter ν in the following way. Let $\mathcal{S}_\epsilon = \{|\xi\rangle : p_A \geq \epsilon\}$ be the set of ϵ -significant eigenkets, i.e., the set of eigenkets for which the subsystem probability $p_A \geq \epsilon$. Since there are $2N$ number of eigenkets, we define:

$$\nu(\epsilon) = \frac{|\mathcal{S}_\epsilon|}{2N}, \quad (5)$$

where $|\mathcal{S}_\epsilon|$ is the number of elements in \mathcal{S}_ϵ , and the argument in $\nu(\epsilon)$ explicitly shows that the parameter ν depends on ϵ . The values of ν can be seen in Fig. 3 for a

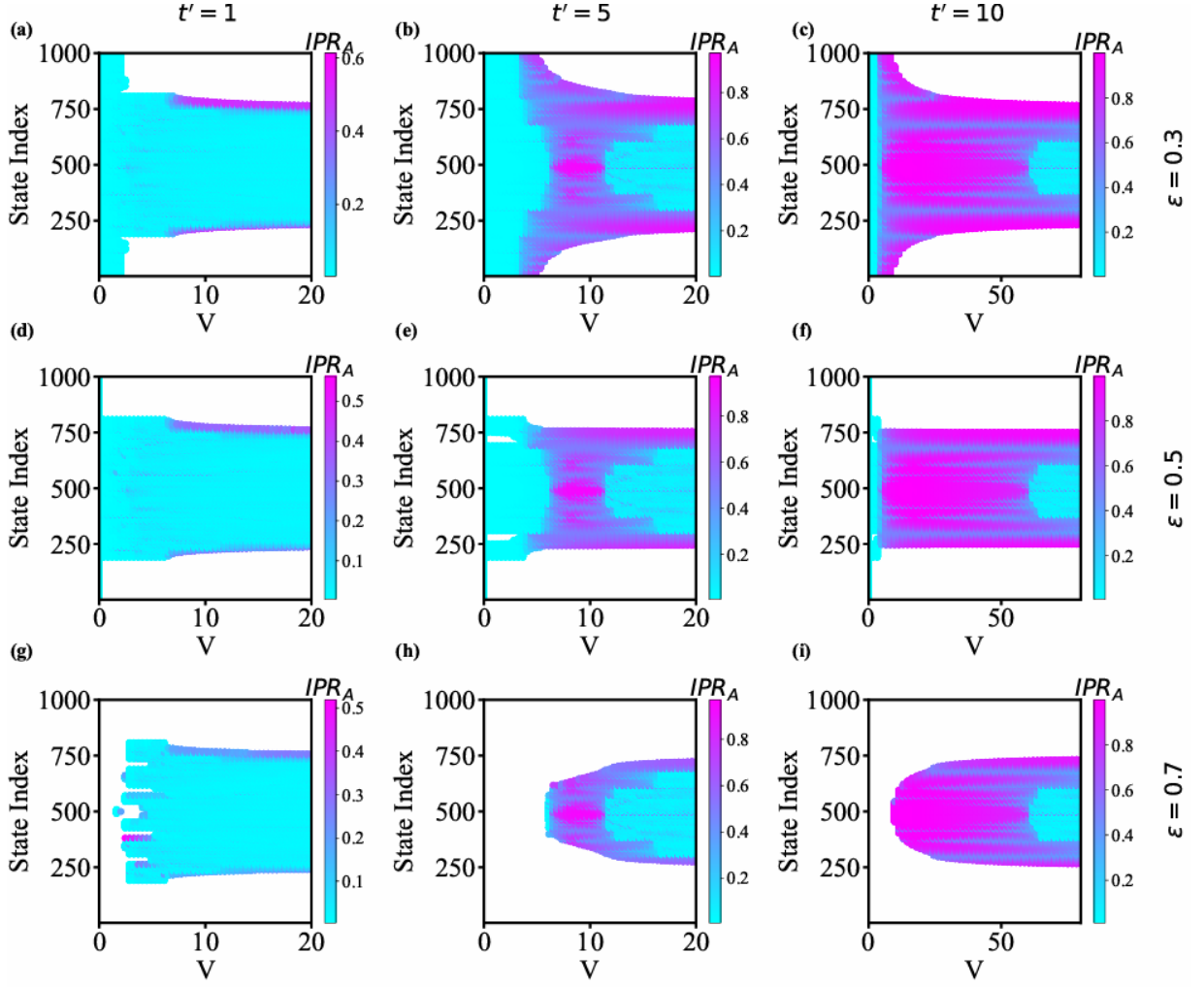


FIG. 4: Plots of IPR_A as function of V for all ϵ -significant states ($\epsilon = 0.3, 0.5$ and 0.7). Calculations are performed for the total subsystem size $N = 500$ and for $t' = 1, 5$ and 10 .

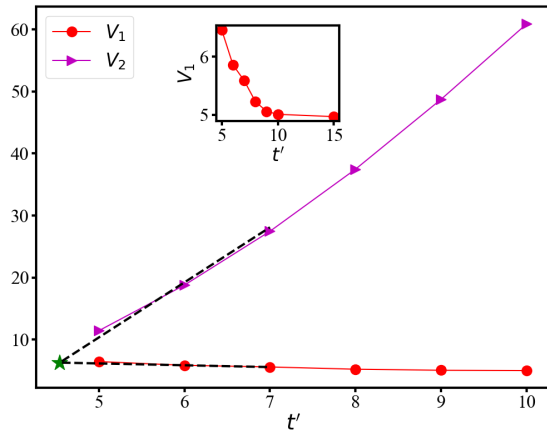


FIG. 5: Variation of V_1 and V_2 as function of t' .

wide range of V and for three fixed values of t' . We get the following main results from this study. For a fixed

value of t' , and for a small value of V , almost all eigenkets are $\epsilon = 0.3$ significant (i.e., $\nu(0.3) = 1$) and almost no eigenket is $\epsilon = 0.7$ significant (i.e., $\nu(0.7) = 0$). As V takes a value beyond a certain threshold (which depends on the given t'), we see that the number of the $\epsilon = 0.3$ significant states decreases (i.e., $\nu(0.3) < 1$), while the number of the $\epsilon = 0.7$ significant states grows (i.e., $\nu(0.7) > 0$). In the very large V limit, $\nu \rightarrow 0.5$ for both the cases. Interestingly, for a wide range of V , we observe that $\nu(0.5)$ is always close to 0.5. This shows that, regardless of the values of t' and V , there are about 50% eigenkets that are $\epsilon = 0.5$ significant for the subsystem A , i.e., for about half of the eigenkets, the subsystem probability $p_A \geq 0.5$.

We can understand the above results in the following way. For a fixed value of t' , and with a low value of V , most of the eigenstates are fully delocalized in the full system. As a result, for the individual eigenkets, $p_A \approx 0.5$. Consequently, $\nu(0.3) \approx 1$, $\nu(0.5) \approx 0.5$ and $\nu(0.7) \approx 0$. Now, as we increase V to a large value, about

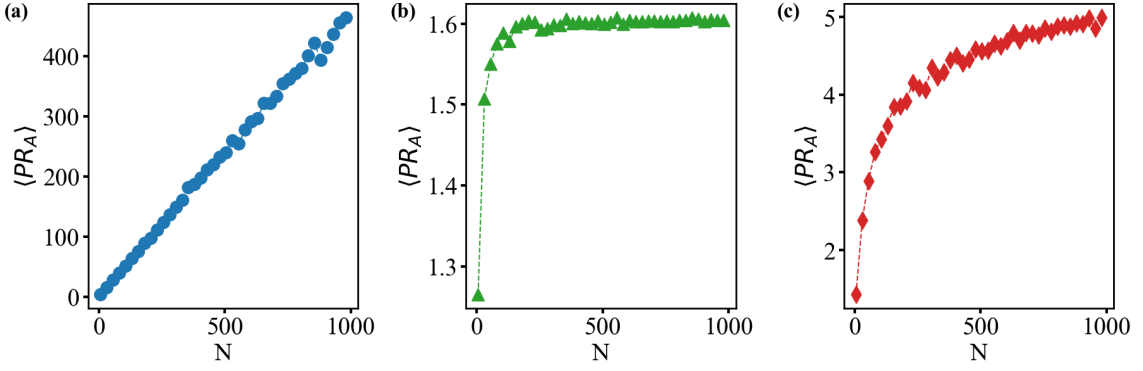


FIG. 6: Plots of $\langle PR_A \rangle$ vs. N for $V = 1, 10, 17$ ($\epsilon = 0.5$ and $t' = 5$).

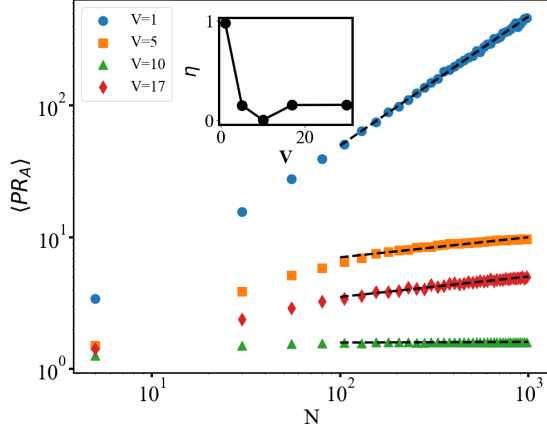


FIG. 7: Log-log plots: $\langle PR_A \rangle$ vs. N for $V = 1, 5, 10, 17$ ($\epsilon = 0.5$ and $t' = 5$). Inset: Scaling exponent (η) vs. V .

half of the eigenkets (approximately N in number) get localized in the bath B . This leaves about N eigenkets that are localized or delocalized in the subsystem A . As a result, for large V , $\nu(0.3) \approx 0.5$, $\nu(0.5) \approx 0.5$ and $\nu(0.7) \approx 0.5$.

To analyze the localization character of the ϵ -significant eigenkets, for example, to see whether an ϵ -significant eigenket is localized within the subsystem A or not, we now compute the inverse participation ratio IPR_A (as in Eq. 3) for these states. Fig. 4 shows the variation of IPR_A as a function of V for different values of ϵ , specifically $\epsilon = 0.3, 0.5$, and 0.7 . These calculations are performed for a total system size $2N = 1000$, considering three different values of t' , namely $t' = 1, 5$, and 10 . The results clearly indicate that for small t' (in particular, $t' = 1$), most of the ϵ -significant eigenkets are not localized within the subsystem A . As we increase t' beyond a critical value t'_c , we see the appearance of a localized phase for intermediate values of V . For a given $t' > t'_c$, and for $V_1 < V < V_2$, almost all the ϵ -significant eigenkets are localized up to a good extent but the states in the middle of the spectrum show stronger localization. For a given t' , we calculate V_1 and V_2 in the following way.

For a state in the middle of the spectrum, we choose V_1 in such a way that $IPR_A < 0.5$ for $V < V_1$ and $IPR_A \geq 0.5$ for $V \geq V_1$. Similarly, for the same state, we choose V_2 in such a way that $IPR_A > 0.5$ for $V < V_2$ and $IPR_A \leq 0.5$ for $V \geq V_2$. The plots for V_1 and V_2 as functions of t' can be seen in Fig. 5. These numerical results also help us find t'_c by extrapolating V_1 and V_2 till they become equal. We estimate that $t'_c \approx 4.6$. It is interesting to note that, as t' increases beyond the critical value t'_c , the value of V_2 increases, while the value of V_1 decreases. The decrease in V_1 with increasing t' can be understood from the fact that, in the limit of very large t' , the subsystem A tends toward a fully localized phase, since the eigenstates are localized along the rungs of the ladder, for any finite V .

The analysis of the subsystem for $V > V_2$ (and $t' > t'_c$) reveals a new phase which we call a weakly delocalized phase with the fractal character. In this parameter regime, some states exhibit delocalization properties (having small IPR_A), while other states (near the edges) are found to be well localized (having large IPR_A). Such reentrance of the delocalized phase at large values of the quasiperiodic potential strength has recently been observed in several one-dimensional models. [47, 48]. To better understand the localization properties of different phases of the subsystem, we next perform the finite size scaling of the average participation ratio, $\langle PR_A \rangle$, where the average is taken only over the ϵ -significant eigenkets:

$$\langle PR_A \rangle = \frac{1}{|\mathcal{S}_\epsilon|} \sum_{n \in \mathcal{S}_\epsilon} \frac{1}{IPR_A^{(n)}}. \quad (6)$$

Here \mathcal{S}_ϵ is the set of the ϵ -significant eigenkets (also see Eq. 5). Fig. 6 shows how $\langle PR_A \rangle$ scales with the subsystem size (N) for $V = 1, 10$ and 17 (for $t' = 5$ and $\epsilon = 0.5$). Corresponding log-log plots, as seen in Fig. 7, demonstrate that the quantity of interest obeys $\langle PR_A \rangle \sim N^\eta$ scaling in general. We find that $\eta = 1$ when $V = 1$ (i.e., when $V < V_1$). This result confirms that the subsystem is in delocalized phase in the regime where V is small. For $V = 10$ (i.e., when $V_1 < V < V_2$), we find $\eta \approx 0$. This shows that the subsystem A is in a localized phase in the intermediate range of V . When $V = 17$ (i.e., when $V > V_2$), we get $\eta < 1$. This indicates that

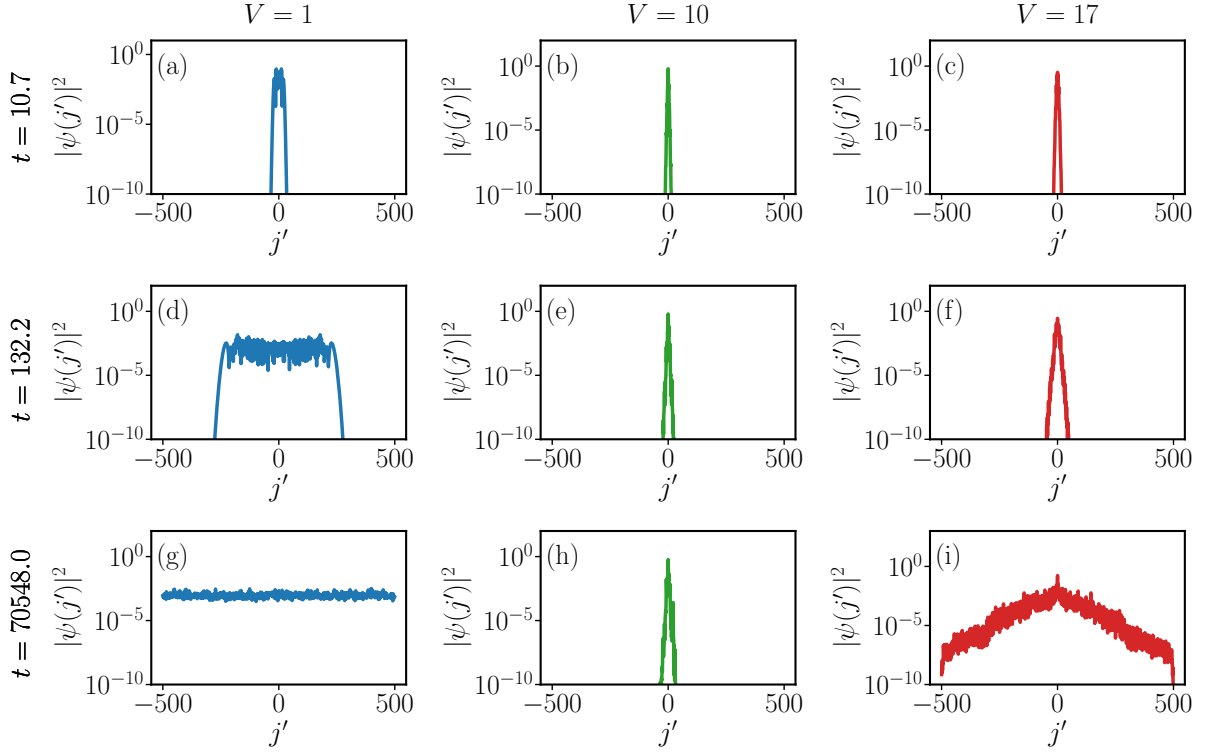


FIG. 8: Probability distribution $|\psi(j')|^2$ vs. j' plot for different V and different instant of time t , for $N = 1000$. The particle is initiated from the middle of the subsystem A , i.e., $j = N/2$, and here $j' = j - N/2$.

the corresponding phase is a fractal. Interestingly, when $V = 5$ (i.e., when V is close to V_1), we also get $\eta < 1$. This observation suggests the presence of a narrow band along the transition line between the delocalized and localized phases, within which the subsystem exhibits a fractal phase.

When $t' < t'_c$, the similar analysis of IPR_A and $\langle PR_A \rangle$ shows that there is no localized phase and we have only two phases - a delocalized phase and weakly delocalized (or fractal) phase. The relevant results may be found in Figs. 15 and 16.

For better understanding of these fractal phases (and other two phases, namely, delocalized and localized phases), we next study the wavepacket dynamics in the subsystem.

IV. DYNAMIC PROPERTIES

In this section, we study the projected wave packet dynamics in subsystem A . We initialize the system by placing one particle at the center of subsystem A , and then let it evolve under the total Hamiltonian H as

$$|\xi(t)\rangle = e^{-iHt}|\phi_0\rangle,$$

where the initial state is given by $|\phi_0\rangle = |1_{N/2}\rangle$.

We focus on the normalized time-evolved state pro-

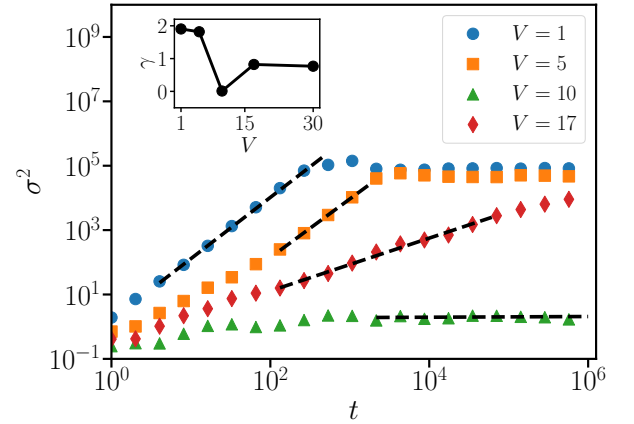


FIG. 9: σ^2 vs t plot for different V for subsystem size $N = 1000$. The black dashed lines show the fitting to the functional form $\sigma^2 \sim t^\gamma$. The inset shows the variation of the exponent γ on V .

jected onto subsystem A , defined as

$$|\psi(t)\rangle = \frac{\hat{P}_A|\xi(t)\rangle}{\|\hat{P}_A|\xi(t)\rangle\|},$$

which is the same as Eq. (2), and study its dynamics.

Here, we first focus on $t' = 5 > t'_c$. Figure 8 shows the time evolution of the probability distribution $|\psi(j, t)|^2 =$

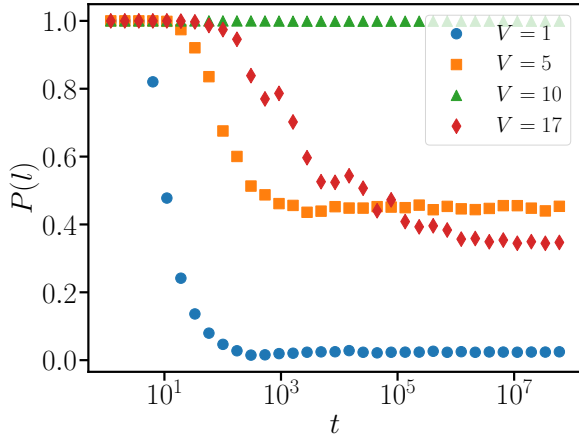


FIG. 10: Variation of $P(l)$, the Probability of finding the particle in the region $N/2 - l$ to $N/2 + l$, with time t for different V . Results are for $N = 1000$ and $l = 10$. Plots are generated using local time averaging to smooth out the data.

$|\langle j|\psi(t)\rangle|^2$ for $V = 1, 10$, and 17 . According to our static results, these three values of V correspond to completely delocalized, completely localized, and weakly delocalized (fractal) phases, respectively. We observe that for $V = 1$, $|\psi(j, t)|^2$ spreads significantly faster across subsystem A compared to the case of $V = 17$. In contrast, for $V = 10$, the probability distribution remains nearly unchanged over time, indicating a fully localized phase.

Next, we quantify the spread of $|\psi(j, t)|^2$ using various measures. We compute the variance σ^2 of this probability distribution, defined as

$$\sigma^2(t) = \sum_{j=1}^N j^2 |\psi(j, t)|^2 - \left[\sum_{j=1}^N j |\psi(j, t)|^2 \right]^2. \quad (7)$$

In Fig. 9, we plot σ^2 as a function of time t for different values of V (with $t' = 5$ fixed). In the completely localized phase (e.g., $V = 10$), we observe that σ^2 remains constant over time, as expected. In contrast, in other regimes, σ^2 grows as $\sigma^2 \sim t^\gamma$ until it saturates due to finite-size effects. For small values of V (e.g., $V = 1$), we find the exponent $\gamma = 2$, indicating ballistic transport. As V increases, we enter a super-diffusive regime where $1 < \gamma < 2$ (see results for $V = 5$), followed by a completely localized phase. Upon further increasing V (e.g., $V = 17$), we enter a weakly delocalized (fractal) regime, as identified in our static calculations, where the dynamics becomes sub-diffusive, i.e., $\gamma < 1$. The variation of the exponent γ with V is shown in the inset of Fig. 9. We have verified the robustness of the exponent γ by varying the system size. An alternative validation of subdiffusive transport, based on the scaling of the projected probability distribution, is presented in Appendix B.

Further, we investigate another measure, $P(l, t)$, de-

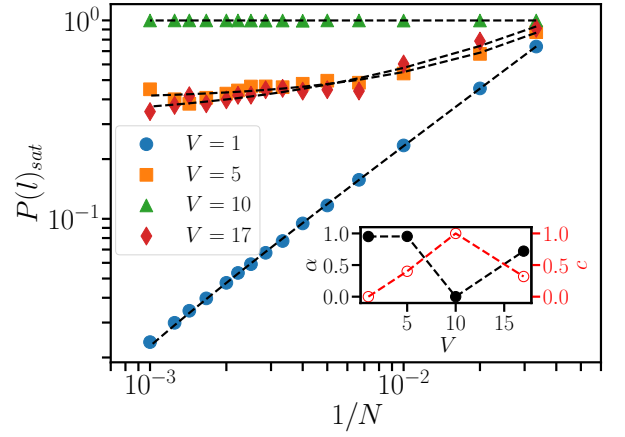


FIG. 11: Scaling of $P(l)_{\text{sat}}$, the long time average of $P(l)$, with inverse of the subsystem size $1/N$. The black dashed line represents the fitting of the data with the functional form $P(l)_{\text{sat}} \sim (1/N)^\alpha + c$. The inset shows the variation of α and c with V . Results are for $2l = 20$.

fined as

$$P(l, t) = \sum_{j=N/2-l}^{N/2+l} |\psi(j, t)|^2, \quad (8)$$

where $l \ll N$. This quantity represents the total probability of finding the particle at time t within a neighborhood of width $2l$ centered around its initial position. For our choice of initial state, we have $P(l, 0) = 1$. This measure provides insight into how much memory of the initial state is retained during the dynamics. In the completely localized phase, one expects $P(l, t) \approx 1$ for all times, provided l is larger than the typical localization length. On the other hand, in a completely delocalized phase, one would expect that at sufficiently large times $|\psi(j, t)|^2 \sim \frac{1}{N}$ for all j , implying that $P(l, t)$ saturates to $P(l) \approx \frac{2l}{N}$. This scales to zero in the thermodynamic limit ($N \rightarrow \infty$), indicating a complete loss of memory of the initial state. Figure 10 confirms this behavior: for $V = 1$ (completely delocalized) and $V = 10$ (completely localized), $P(l = 10, t)$ behaves as expected—decreasing rapidly with time and saturating to a small value for $V = 1$, while remaining close to 1 for all times in the case of $V = 10$. Interestingly, for $V = 5$ and $V = 17$, $P(l, t)$ decreases at early times but saturates to a significantly higher value than in the delocalized case ($V = 1$), indicating partial memory retention.

To investigate further whether the initial memory persists in the thermodynamic limit, we perform a finite-size scaling analysis of the long-time averaged value of $P(l, t)$, defined as

$$P(l)_{\text{sat}} = \lim_{T \rightarrow \infty} \frac{1}{T} \int_0^T P(l, t) dt. \quad (9)$$

Figure 11 shows the scaling of $P(l)_{\text{sat}}$ with subsystem size N for different values of V . We fit the data using

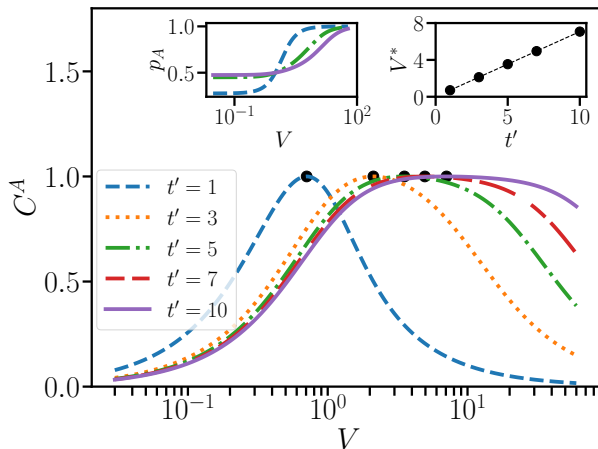


FIG. 12: A localization measure C^A vs. V plots for the mid-spectrum state of H_T for different t' . One inset shows the probability of a particle being at subsystem p_A vs. V for the same state. The top-right inset shows the scaling of V^* (the V for which C^A attains a peak) with t' .

the function $\text{const}/N^\alpha + c$, and the variation of the fitting parameters α and c with V is shown in the inset of Fig. 11. In the completely delocalized phase ($V = 1$), we find $\alpha \approx 1$ and $c \approx 0$, as expected. In the completely localized phase, $P(l)_{\text{sat}}$ remains nearly constant with N . Interestingly, for $V = 5$ (super-diffusive regime) and $V = 17$ (sub-diffusive regime), the scaling behavior is similar, but the fitted constant $c \neq 0$ in both cases. This indicates that a finite portion of the initial state's memory survives even in the thermodynamic limit. We investigate $t' = 3 < t'_c$ case in the Appendix. C, and find no signature of the localized phase; instead the dynamics suggest a ballistic (for small V) and a subdiffusive phase (for large V), with an intermediate crossover regime which can be either super- or subdiffusive in nature.

V. ANALYTICAL UNDERSTANDING OF RESULTS

A. Toy model

Here, we propose a minimal toy model to help understand some of the numerical results obtained for the Hamiltonian in Eq. (1). One surprising observation from our numerical simulations is the reentrance of the delocalized phase with increasing V . Typically, at least for $t' = 0$, increasing V tends to promote localization in subsystem B. It is therefore natural to expect that introducing a nonzero t' would further localize subsystem A as V increases. Contrary to this expectation, we find that beyond a certain threshold (that depends on t'), increasing V leads to the reappearance of the delocalized phase.

To investigate this phenomenon, we study a minimal toy model described by the Hamiltonian (using the same site indexing as shown in the schematic Fig. 1),

$$H_T = -(c_1^\dagger c_2 + t' c_1^\dagger c_3 + t' c_2^\dagger c_4 + hc) + V(c_3^\dagger c_3 - c_4^\dagger c_4), \quad (10)$$

with the aim of capturing the mechanism behind the reentrance of the delocalized phase. If $t' = 0$, the A and B parts of the system are completely decoupled, and the eigenstates (specifically, two of them) remain entirely on the B part of the system and are fully localized. In contrast, for the other two eigenstates that lie entirely within the A part, the probability of finding the particle on sites 1 and 2 remains equal. If one introduces a finite t' and investigates how this scenario evolves with varying V , to quantify the degree of delocalization of an eigenstate within subsystem A (which consists only of sites 1 and 2), we define the following measure for an eigenstate $|\xi\rangle$:

$$C^A = \frac{||\langle 1|\xi\rangle|^2 - |\langle 2|\xi\rangle|^2|}{|\langle 1|\xi\rangle|^2 + |\langle 2|\xi\rangle|^2}. \quad (11)$$

Now, among the two sites in A, if $|\xi\rangle$ is completely localized on only one of the sites (either at site 1 or 2), then $C^A = 1$, and on the other hand, if it is completely delocalized (probabilities to be at site 1 and 2 are equal), then $C^A = 0$. Given H_T is a 4×4 matrix, C^A can be obtained analytically, and for the mid-spectrum state,

$$C^A = \frac{|(y - V)^2 - (y^2 - Vy - t'^2)^2|}{(y - V)^2 + (y^2 - Vy - t'^2)^2}, \quad (12)$$

where, $x = \sqrt{\frac{V^2}{2} + t'^2 + \frac{\sqrt{V^4 + 4V^2 t'^2 - 2V^2 + 4t'^2 + 1}}{2}} + \frac{1}{2}$, and $y = \sqrt{\frac{V^2}{2} + t'^2 - \frac{\sqrt{V^4 + 4V^2 t'^2 - 2V^2 + 4t'^2 + 1}}{2}} + \frac{1}{2}$.

Figure 12 (main panel) shows the variation of C^A with V for different values of t' . As V increases, C^A initially increases, reaches a peak at $V = V^*$, and then decreases as V continues to grow. This behavior closely mimics the reentrance phenomenon of delocalization observed in the original Hamiltonian H . We also obtain the analytical expression $V^* = \frac{t'}{\sqrt{2}}$ by solving the equation $\frac{dC^A}{dV}|_{V^*} = 0$.

The inset of Fig. 12 shows the variation of the total probability that the particle remains in subsystem A for the eigenstate $|\xi\rangle$, given by

$$p_A = |\langle 1|\xi\rangle|^2 + |\langle 2|\xi\rangle|^2, \quad (13)$$

as a function of V . We find that as V increases, this probability approaches 1, indicating that the state becomes increasingly localized within subsystem A, making it a significant state for our analysis of subsystem A.

B. Effective model for the subsystem

We will see here that a model closely related to ours (Eq. 1) can be reduced to a simple effective model for

the subsystem. The model we consider here does not have the hopping term along the B leg (the bath). The Hamiltonian of this model is the same as the one appears in Eq. 1 with $t_B = 0$. The two models are expected to give similar results in the large t' and V limits.

Consider that $\psi = \sum_{j=1}^N a_j |A_j\rangle + \sum_{i'=1}^N b_{i'} |B_{i'}\rangle$ is an eigenstate of the Hamiltonian of the current model (where $t_B = 0$). Here $|A_j\rangle$ and $|B_{i'}\rangle$ are the site basis of subsystem A and bath B , respectively, and a_j and $b_{i'}$ are the corresponding coefficients. It may be noted that the index i' corresponds to $N+i$ in the original Hamiltonian in Eq. 1. If E is the eigenvalue associated with ψ , then

$$-t'a_n + V_nb_n = Eb_n \quad (14)$$

$$-t_A a_{n+1} - t_A a_{n-1} - t'b_n = Ea_n \quad (15)$$

Here $V_n = V \cos(2\pi\beta n + \phi)$, the AA potential as appears in Eq. 1. From Eq. 14, we get:

$$b_n = \frac{-t'a_n}{(E - V_n)}.$$

We use this expression to replace b_n in Eq. 15; this yields:

$$-t_A a_{n+1} - t_A a_{n-1} + \frac{(t')^2 a_n}{(E - V_n)} = Ea_n. \quad (16)$$

One can recast this equation in the following form:

$$-t_A a_{n+1} - t_A a_{n-1} + V_n^{eff} a_n = E^{eff} a_n. \quad (17)$$

Here, $E^{eff} = E - 1/\alpha$ and

$$V_n^{eff} = \frac{\lambda \cos(2\pi\beta n + \phi)}{1 - \lambda\alpha \cos(2\pi\beta n + \phi)},$$

with $\lambda = V(t')^2/E^2$ and $\alpha\lambda = V/E$.

We therefore see that the subsystem A of our model (with $t_B = 0$) effectively behaves as a generalized Aubrey-André (GAA) one-dimensional chain, which also exhibit similar ballistic, superdiffusive, and subdiffusive phases, as reported recently in Ref. [49].

VI. CONCLUSION

In summary, in this work, we study a two-leg ladder model, where one leg (called bath) is described by an AA-type Hamiltonian (which can undergo a localization-delocalization transition by tuning the strength of the incommensurate potential) and the other leg by the usual nearest-neighbor tight-binding model, which we refer to as the subsystem. By introducing the coupling t' between these two legs, we obtain a rich phase diagram as shown schematically in Fig. 2. We notice that beyond a critical coupling strength t'_c , there exists a regime where the subsystem can be completely localized. Also, we find different parameter regimes where the transport can be

ballistic, subdiffusive, and superdiffusive in nature. However, it is important to note that there is an intermediate region, labeled as P4 phase in Fig. 2, where the subsystem exhibits a complex phase structure. Here it may show super- or subdiffusive behavior based on parameter values and time scale of investigation. A more detailed study is required to gain better insight into the nature of phases in this crossover region. We further explain some of these results using a toy model and also by mapping it to a well-studied 1D GAA model.

Our study has two primary implications: 1) it partially addresses the question of whether a localized bath can localize the system attached to it. At least in the non-interacting limit, our study finds that it is possible to have a suitable parameter regime where the bath can localize the system. 2) By doing this analysis, we also demonstrate a way to control the dynamics of a system (here, it is subsystem A) by not explicitly disturbing the system directly; instead, we have achieved that by altering another system (here, it is the bath B) and its coupling with A . This can have a significant application in quantum technologies and can potentially be implemented in experiments [33, 34].

ACKNOWLEDGMENTS

R.M. acknowledges the DST-Inspire research grant by the Department of Science and Technology, Government of India.

Appendix A: Results for random cosine model

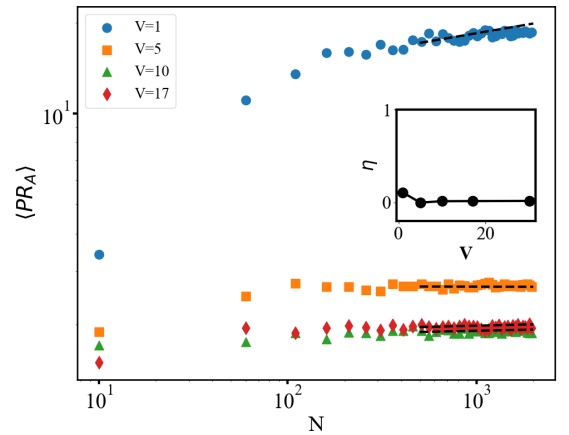


FIG. 13: Log-log plot of disordered averaged $\langle PR_A \rangle$ vs N for $V = 1, 5, 10, 17$ ($\epsilon = 0.5$ and $t' = 5$). Inset: Scaling exponent (η) vs. V .

Instead of the correlated AA type disorder, if we take a random disorder in bath B , then the phase structure of the subsystem A is expected to be completely different. To verify this, we replace the uniform phase factor ϕ in

Eq. 1 by a random site-dependent phase ϕ_i . We then calculate $\langle PR_A \rangle$ (averaged over multiple realizations of ϕ_i) as function of the subsystem size (N). The results may be found in Fig. 13. Fitting of the data by $\langle PR_A \rangle \sim N^\eta$ shows that the exponent (η) is very small regardless of the value of V . This indicates that a random (uncorrelated) potential in bath B localizes all states in the subsystem A ; this is in accordance with what is expected from the Anderson localization in one-dimensional system [1].

Appendix B: Scaling of projected probability distribution

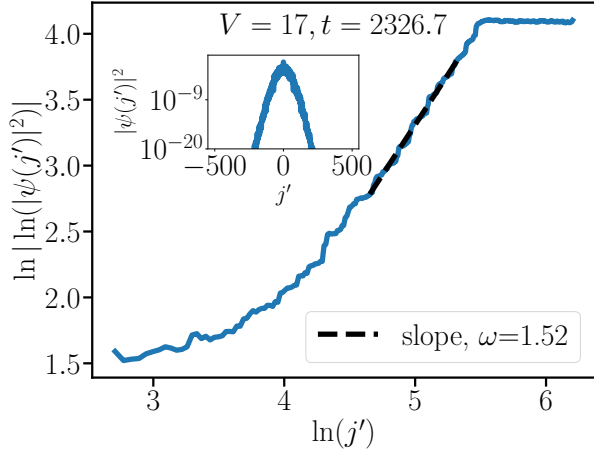


FIG. 14: $\ln |\ln(|\psi(j')|^2)|$ vs. $\ln(j')$ plot for $j' > 0$ for $V = 17$ and $N = 1000$. The dashed line corresponds to the best fit with slope $\omega = 1.52$. The inset shows the probability distribution $|\psi(j')|^2$ vs. j' , where $j' = j - N/2$.

It has been argued recently in Ref. [50] that if the transport is sub (super) diffusive, the probability distribution at large time will have a stretched-exponential form. Moreover, that stretched exponent is related to the scaling exponent γ ; note $\sigma^2 \sim t^\gamma$. In our context, if one starts from the same initial state $|\phi_0\rangle = |1_{N/2}\rangle$ as mentioned in the main text, the probability distribution corresponding to the projected state in A obeys the following scaling form in the large t and $j' = j - N/2$ limit,

$$|\psi(j', t)|^2 \sim a(t)e^{-b(t)|j'|^\omega} \quad (\text{B1})$$

where $a(t)$ and $b(t)$ are functions of t , and $\omega = \frac{2}{2-\gamma}$ (see Ref. [50]). Here, we obtain the scaling exponent $\omega = 1.52$ by fitting $|\psi(j', t)|^2$ with j' for $V = 17$ and for large enough t (see Fig. 14). It implies $\gamma \approx 0.7 < 1$; sub-diffusive transport, precisely what we have observed in the main text.

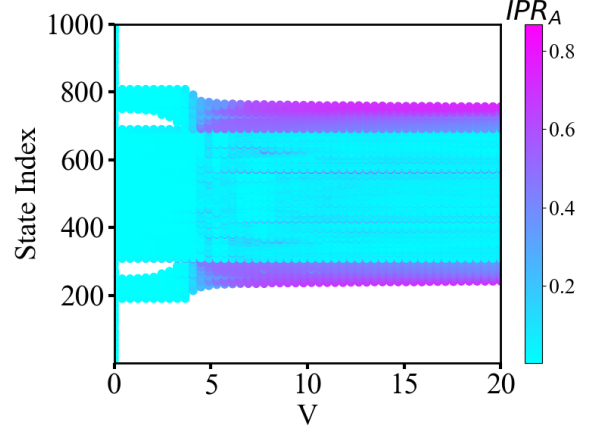


FIG. 15: Variation of IPR_A with V for all ϵ -significant states. Calculations are performed for the total subsystem size $N = 500$, $t' = 3$ and $\epsilon = 0.5$

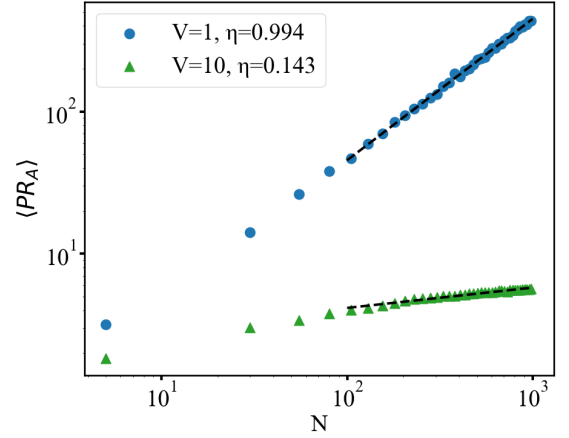


FIG. 16: $\langle PR_A \rangle$ vs. N plot for $t' = 3$ at $V = 1$ and $V = 10$.

Appendix C: Understanding Phases for $t' < t'_c$

We note that our subsystem A is in a fully delocalized (or in ballistic) phase when $t' = 0$ (irrespective of the value of V). We also have analyzed phases of the system when $t' > t'_c$ ($t'_c \approx 4.6$). In this Appendix, we present results for $0 < t' < t'_c$. For definiteness, we focus on results corresponding to $t' = 3$.

We have calculated IPR_A for $\epsilon = 0.5$, and $t' = 3$; we do not observe any localized region in the intermediate V values. Corresponding results can be found in Fig. 15. A similar behavior has been observed for $t' = 4$. We have further analyzed the scaling behavior of disorder-averaged $\langle PR_A \rangle$ at different V regions. The $\langle PR_A \rangle$ vs. N plot 16 suggests that at very low V , the subsystem A is completely delocalized, but if we increase V , we will see only a few states at the edge that are becoming strongly localized. However, the middle states always remain delocalized (even in larger V). The scaling exponent of $\langle PR_A \rangle$

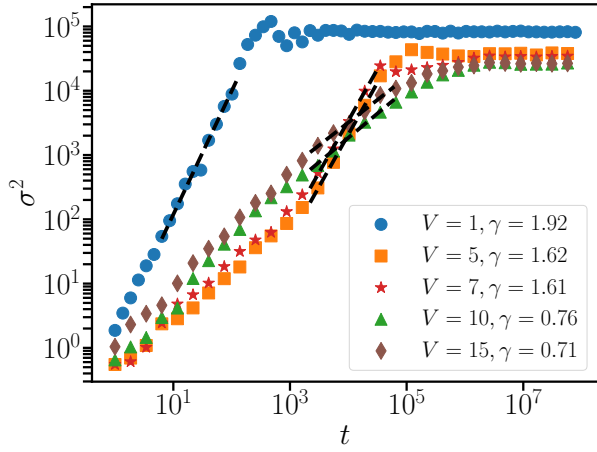


FIG. 17: σ^2 vs t plot for different V , but for fixed $t' = 3$ and subsystem size $N = 1000$. The black dashed line shows the fitting to the functional form $\sigma^2 \sim t^\gamma$.

reveals that the middle states do not have the same degree of delocalization at $V = 1$ and $V = 10$. States at $V = 10$ are much weakly delocalized compared to $V = 1$.

We have also investigated the dynamical properties of the subsystem for $t' = 3$. Fig. 17 shows for $V = 1$, $\gamma \sim 2$, which is a signature of ballistic growth; on the other hand, unlike $t' = 5$, in this case for $V = 10$, we see a subdiffusive growth as the exponent $\gamma = 0.76$. In the intermediate regime, we also find a superdiffusive regime (see $V = 5$ and $V = 7$ data), where $1 < \gamma < 2$.

-
- [1] P. W. Anderson, Absence of diffusion in certain random lattices, *Phys. Rev.* **109**, 1492 (1958).
 - [2] E. Abrahams, P. W. Anderson, D. C. Licciardello, and T. V. Ramakrishnan, Scaling theory of localization: Absence of quantum diffusion in two dimensions, *Phys. Rev. Lett.* **42**, 673 (1979).
 - [3] P. A. Lee and T. V. Ramakrishnan, Disordered electronic systems, *Rev. Mod. Phys.* **57**, 287 (1985).
 - [4] M. Žnidarič, T. c. v. Prosen, and P. Prelovšek, Many-body localization in the heisenberg xxz magnet in a random field, *Phys. Rev. B* **77**, 064426 (2008).
 - [5] D. A. Abanin, E. Altman, I. Bloch, and M. Serbyn, Colloquium: Many-body localization, thermalization, and entanglement, *Rev. Mod. Phys.* **91**, 021001 (2019).
 - [6] A. Pal and D. A. Huse, Many-body localization phase transition, *Phys. Rev. B* **82**, 174411 (2010).
 - [7] J. H. Bardarson, F. Pollmann, and J. E. Moore, Unbounded growth of entanglement in models of many-body localization, *Phys. Rev. Lett.* **109**, 017202 (2012).
 - [8] D. J. Luitz, N. Laflorencie, and F. Alet, Many-body localization edge in the random-field heisenberg chain, *Phys. Rev. B* **91**, 081103 (2015).
 - [9] D. M. Basko, I. L. Aleiner, and B. L. Altshuler, Metal-insulator transition in a weakly interacting many-electron system with localized single-particle states, *Annals of physics* **321**, 1126 (2006).
 - [10] R. Nandkishore and D. A. Huse, Many-body localization and thermalization in quantum statistical mechanics, *Annu. Rev. Condens. Matter Phys.* **6**, 15 (2015).
 - [11] S. Ghosh, A. Acharya, S. Sahu, and S. Mukerjee, Many-body localization due to correlated disorder in fock space, *Physical Review B* **99**, 165131 (2019).
 - [12] J. M. Deutsch, Quantum statistical mechanics in a closed system, *Phys. Rev. A* **43**, 2046 (1991).
 - [13] M. Srednicki, Chaos and quantum thermalization, *Phys. Rev. E* **50**, 888 (1994).
 - [14] M. Rigol and M. Srednicki, Alternatives to eigenstate thermalization, *Physical review letters* **108**, 110601 (2012).
 - [15] M. Rigol, Breakdown of thermalization in finite one-dimensional systems, *Physical review letters* **103**, 100403 (2009).
 - [16] A. Morningstar, L. Colmenarez, V. Khemani, D. J. Luitz, and D. A. Huse, Avalanches and many-body resonances in many-body localized systems, *Phys. Rev. B* **105**, 174205 (2022).
 - [17] D. Sels, Bath-induced delocalization in interacting disordered spin chains, *Phys. Rev. B* **106**, L020202 (2022).
 - [18] J. Šuntajs, J. Bonča, T. c. v. Prosen, and L. Vidmar, Quantum chaos challenges many-body localization, *Phys. Rev. E* **102**, 062144 (2020).
 - [19] S. Aubry and G. André, Analyticity breaking and anderson localization in incommensurate lattices, *Ann. Israel Phys. Soc* **3**, 18 (1980).
 - [20] B. Hetényi and I. Balogh, Localization at irrational fillings in the aubry-andré model, *arXiv preprint arXiv:2409.01233* (2024).
 - [21] B. Hetényi, Scaling of the bulk polarization in extended and localized phases of a quasiperiodic model, *Phys. Rev. B* **110**, 125124 (2024).
 - [22] M. Suman, S. Aravinda, and R. Modak, Probing quantum phase transitions via quantum speed limits, *Phys. Rev. A* **110**, 012466 (2024).
 - [23] A. Sahoo, U. Mishra, and D. Rakshit, Localization-driven quantum sensing, *Phys. Rev. A* **109**, L030601 (2024).
 - [24] A. Goswami, Emergence of single-particle mobility edge (spme) in a ladder network under a modified aubrey-andré-harper (aah) kind distortion, *arXiv preprint arXiv:2502.01511* (2025).
 - [25] Y. Wang, X. Xia, L. Zhang, H. Yao, S. Chen, J. You, Q. Zhou, and X.-J. Liu, One-dimensional quasiperiodic mosaic lattice with exact mobility edges, *Phys. Rev. Lett.* **125**, 196604 (2020).
 - [26] X. Li and S. Das Sarma, Mobility edge and intermediate phase in one-dimensional incommensurate lattice potentials, *Phys. Rev. B* **101**, 064203 (2020).
 - [27] M. Rossignolo and L. Dell'Anna, Localization transitions and mobility edges in coupled aubry-andré chains, *Phys.*

- Rev. B **99**, 054211 (2019).
- [28] J. D. Bodyfelt, D. Leykam, C. Danieli, X. Yu, and S. Flach, Flatbands under correlated perturbations, *Phys. Rev. Lett.* **113**, 236403 (2014).
 - [29] C. M. Soukoulis and E. N. Economou, Localization in one-dimensional lattices in the presence of incommensurate potentials, *Phys. Rev. Lett.* **48**, 1043 (1982).
 - [30] S. Gopalakrishnan, Self-dual quasiperiodic systems with power-law hopping, *Phys. Rev. B* **96**, 054202 (2017).
 - [31] J. Biddle and S. Das Sarma, Predicted mobility edges in one-dimensional incommensurate optical lattices: An exactly solvable model of anderson localization, *Phys. Rev. Lett.* **104**, 070601 (2010).
 - [32] S. Ganeshan, J. H. Pixley, and S. Das Sarma, Nearest neighbor tight binding models with an exact mobility edge in one dimension, *Phys. Rev. Lett.* **114**, 146601 (2015).
 - [33] T. Kohlert, S. Scherg, X. Li, H. P. Lüschen, S. Das Sarma, I. Bloch, and M. Aidelsburger, Observation of many-body localization in a one-dimensional system with a single-particle mobility edge, *Phys. Rev. Lett.* **122**, 170403 (2019).
 - [34] H. P. Lüschen, S. Scherg, T. Kohlert, M. Schreiber, P. Bordia, X. Li, S. Das Sarma, and I. Bloch, Single-particle mobility edge in a one-dimensional quasiperiodic optical lattice, *Phys. Rev. Lett.* **120**, 160404 (2018).
 - [35] M. Schreiber, S. S. Hodgman, P. Bordia, H. P. Lüschen, M. H. Fischer, R. Vosk, E. Altman, U. Schneider, and I. Bloch, Observation of many-body localization of interacting fermions in a quasirandom optical lattice, *Science* **349**, 842 (2015).
 - [36] F. A. An, K. Padavić, E. J. Meier, S. Hegde, S. Ganeshan, J. H. Pixley, S. Vishveshwara, and B. Gadway, Interactions and mobility edges: Observing the generalized aubry-andré model, *Phys. Rev. Lett.* **126**, 040603 (2021).
 - [37] R. Modak and S. Mukerjee, Many-body localization in the presence of a single-particle mobility edge, *Phys. Rev. Lett.* **115**, 230401 (2015).
 - [38] X. Li, S. Ganeshan, J. H. Pixley, and S. Das Sarma, Many-body localization and quantum nonergodicity in a model with a single-particle mobility edge, *Phys. Rev. Lett.* **115**, 186601 (2015).
 - [39] D.-L. Deng, S. Ganeshan, X. Li, R. Modak, S. Mukerjee, and J. Pixley, Many-body localization in incommensurate models with a mobility edge, *Annalen der Physik* **529**, 1600399 (2017).
 - [40] R. Modak, S. Ghosh, and S. Mukerjee, Criterion for the occurrence of many-body localization in the presence of a single-particle mobility edge, *Phys. Rev. B* **97**, 104204 (2018).
 - [41] S. Nag and A. Garg, Many-body mobility edges in a one-dimensional system of interacting fermions, *Phys. Rev. B* **96**, 060203 (2017).
 - [42] R. Nandkishore, Many-body localization proximity effect, *Phys. Rev. B* **92**, 245141 (2015).
 - [43] K. Hyatt, J. R. Garrison, A. C. Potter, and B. Bauer, Many-body localization in the presence of a small bath, *Phys. Rev. B* **95**, 035132 (2017).
 - [44] P. Brighi, M. Ljubotina, D. A. Abanin, and M. Serbyn, Many-body localization proximity effect in a two-species bosonic hubbard model, *Phys. Rev. B* **108**, 054201 (2023).
 - [45] S.-H. Chiew, J. Gong, L.-C. Kwek, and C.-K. Lee, Stability and dynamics of many-body localized systems coupled to a small bath, *Phys. Rev. B* **107**, 224202 (2023).
 - [46] A. Rubio-Abadal, J.-y. Choi, J. Zeiher, S. Hollerith, J. Rui, I. Bloch, and C. Gross, Many-body delocalization in the presence of a quantum bath, *Phys. Rev. X* **9**, 041014 (2019).
 - [47] S. Roy, T. Mishra, B. Tanatar, and S. Basu, Reentrant localization transition in a quasiperiodic chain, *Phys. Rev. Lett.* **126**, 106803 (2021).
 - [48] S. Roy, S. Chattopadhyay, T. Mishra, and S. Basu, Critical analysis of the reentrant localization transition in a one-dimensional dimerized quasiperiodic lattice, *Phys. Rev. B* **105**, 214203 (2022).
 - [49] S. Banerjee, S. R. Padhi, and T. Mishra, Emergence of distinct exact mobility edges in a quasiperiodic chain, *arXiv preprint arXiv:2503.19834* (2025).
 - [50] F. Cecconi, G. Costantini, A. Taloni, and A. Vulpiani, Probability distribution functions of sub- and superdiffusive systems, *Phys. Rev. Res.* **4**, 023192 (2022).
 - [51] A. Purkayastha, S. Sanyal, A. Dhar, and M. Kulkarni, Anomalous transport in the aubry-andré-harper model in isolated and open systems, *Phys. Rev. B* **97**, 174206 (2018).
 - [52] N. C. Murphy, R. Wortis, and W. A. Atkinson, Generalized inverse participation ratio as a possible measure of localization for interacting systems, *Phys. Rev. B* **83**, 184206 (2011).